Fast and slow voltage sensor rearrangements during activation gating in Kv1.2 channels detected using tetramethylrhodamine fluorescence

Andrew James Horne,[1] Christian Joseph Peters,[2] Thomas William Claydon,[1] and David Fedida[1]

[1]Department of Anesthesiology, Pharmacology, and Therapeutics and [2]Department of Cellular and Physiological Sciences, University of British Columbia, Vancouver, British Columbia V6T 1Z3, Canada

The Kv1.2 channel, with its high resolution crystal structure, provides an ideal model for investigating conformational changes associated with channel gating, and fluorescent probes attached at the extracellular end of S4 are a powerful way to gain a more complete understanding of the voltage-dependent activity of these dynamic proteins. Tetramethylrhodamine-5-maleimide (TMRM) attached at A291C reports two distinct rearrangements of the voltage sensor domains, and a comparative fluorescence scan of the S4 and S3–S4 linker residues in *Shaker* and Kv1.2 shows important differences in their emission at other homologous residues. Kv1.2 shows a rapid decrease in A291C emission with a time constant of 1.5 ± 0.1 ms at 60 mV ($n = 11$) that correlates with gating currents and reports on translocation of the S4 and S3–S4 linker. However, unlike any Kv channel studied to date, this fast component is dwarfed by a larger, slower quenching of TMRM emission during depolarizations between −120 and −50 mV (τ = 21.4 ± 2.1 ms at 60 mV, $V_{1/2}$ of −73.9 ± 1.4 mV) that is not seen in either *Shaker* or Kv1.5 and that comprises >60% of the total signal at all activating potentials. The slow fluorescence relaxes after repolarization in a voltage-dependent manner that matches the time course of Kv1.2 ionic current deactivation. Fluorophores placed directly in S1 and S2 at I187 and T219 recapitulate the time course and voltage dependence of slow quenching. The slow component is lost when the extracellular S1–S2 linker of Kv1.2 is replaced with that of Kv1.5 or *Shaker*, suggesting that it arises from a continuous internal rearrangement within the voltage sensor, initiated at negative potentials but prevalent throughout the activation process, and which must be reversed for the channel to close.

The Journal of General Physiology

INTRODUCTION

Voltage-gated potassium channels, or Kv channels, comprise a large class of membrane-spanning proteins involved in mediating the recovery of excitable cells from depolarizing stimuli. Because of recent success in crystallizing various forms of potassium channels, they have been used as structural models for many other channels. Crystal structures from Kv1.2 (Long et al., 2005a,b) and a Kv1.2/Kv2.1 chimera channel (Long et al., 2007) show the voltage sensor and pore domains as being separate from one another, coupled mechanically via the S4–S5 linker and structurally by associations between the extracellular region of S1 and residues in the P-loop helix (Lee et al., 2009). Crystallographic modeling of protein conformation has gone a long way toward helping us understand coupling between the voltage sensor and pore domains and provided ideas of how less structurally defined components of the channel, particularly the transmembrane linker segments, may be oriented. Yet, it is still often difficult to understand the real-time changes in channel structure that occur during opening and closing (gating) from these structural models.

Fluorescence studies, on the other hand, can provide time-resolved measurements of transmembrane domain movement, and these can be interpreted along with ionic and gating current recordings made simultaneously. When a fluorescent probe is linked to a cysteine introduced at the extracellular end of S4 in both *Shaker* (A359C) and Kv1.5 (A397C), the time course and voltage dependence of gating charge movement during depolarization matches the fluorescence quenching and fluorescence-voltage relationships (Mannuzzu et al., 1996; Cha and Bezanilla, 1997; Claydon et al., 2007b; Vaid et al., 2008), suggesting that rapid changes in fluorescence reflect conformational changes at the outer end of S4 that underlie Kv activation gating. Fluorophores in S4 in both channels also consistently report secondary changes in fluorescence emission that correlate with events occurring in the pore domain, like inactivation (Loots and Isacoff, 1998; Claydon et al., 2007a; Vaid et al., 2008). Although the transmembrane domains of potassium channels are well conserved among all families in terms of primary and secondary sequence (Doyle et al., 1998; Jiang et al., 2003; Long et al., 2005a), the nature of the secondary fluorescence differs, suggesting

Correspondence to David Fedida: fedida@interchange.ubc.ca

T.W. Claydon's present address is Dept. of Biomedical Physiology and Kinesiology, Simon Fraser University, Burnaby, British Columbia V5A 1S6, Canada.

Abbreviations used in this paper: PMT, photomultiplier tube; TMRM, tetramethylrhodamine-5-maleimide; WT, wild type.

The Rockefeller University Press $30.00
J. Gen. Physiol. Vol. 136 No. 1 83–99
www.jgp.org/cgi/doi/10.1085/jgp.201010413

that there may be dynamic differences between the pore and/or voltage sensor domain interactions of Kv1 channels arising from differences in channel structure/gating. Voltage clamp fluorimetry has recently been applied to the study of other Kv channels, such as K_{Ca} (Savalli et al., 2006), human ether a-go-go related gene (Smith and Yellen, 2002), Kv1.5 (Vaid et al., 2008), and Kv1.2 (Peters et al., 2009).

The high resolution structure of Kv1.2 provides an ideal model to further explore differences in Kv1.x gating. In this paper, we have undertaken the first detailed examination of gating current and fluorescence measurements in the Kv1.2 voltage sensor. Tetramethylrhodamine-5-maleimide (TMRM) labeled at the externally accessible A291C residue in S4 (Fig. 1) exhibits a fast quenching component that correlates with the time course and voltage dependence of gating charge movement. In addition, Kv1.2 A291C-TMRM and other residues in the S3–S4 linker, unlike all other voltage-gated channels studied, also detect a second and much slower quenching that represents up to 60% of the total fluorescence change. Through the use of chimera channels and fluorophores placed within S1 and S2, we suggest that this slow phase may report rearrangements of voltage sensor moieties other than S4. The reversal of slow rearrangements may be required for the channel to deactivate, suggesting that they play an important role in determining the stability of the open channel. Our findings are interpreted in the context of the channel structures in the activated state (Long et al., 2005a, 2007) and computer modeling of the closed state (Yarov-Yarovoy et al., 2006; Pathak et al., 2007).

MATERIALS AND METHODS

Molecular biology and RNA preparation

Shaker and Kv1.2 constructs were expressed in *Xenopus laevis* oocytes using a modified pBluescript SKII expression vector (pEXO; a gift from A. Sivaprasadarao, University of Leeds, Leeds, England, United Kingdom). An N-terminal–deleted, fast inactivation–removed mutant, Δ6-46 (*Shaker-IR*) (Hoshi et al., 1991), with the lone externally accessible endogenous cysteine removed (C245V) was used as the base construct for all subsequent *Shaker* mutations. Cysteine residues were introduced through site-directed mutagenesis. Oligonucleotide primers were synthesized by either Sigma-Aldrich or Integrated DNA Technologies, and mutations were generated using the QuikChange kit (Agilent Technologies). Successful mutations were confirmed by sequencing the constructs using the core facility unit at the University of British Columbia. cRNA was synthesized from linear cDNA using a cRNA transcription kit (mMessage mMachine T7 Ultra; Applied Biosystems). Kv1.5–Kv1.2 chimera channels were made as previously described (Rezazadeh et al., 2007). In brief, PCR amplification of the desired segment of Kv1.2 was used to introduce either a PmlI (Kv1.5-S12L-Kv1.2) or ClaI (Kv1.5-S23L-Kv1.2) restriction enzyme site. Kv1.5 cDNA was then subcloned into the Kv1.2 channel using the specified enzyme and EcoRI. Constructs were further subcloned into a pBluescript SK^+ vector using HindIII and EcoRI restriction sites. The A291C mutation was made and sequenced as described above. For construction of the *Shaker*-Kv1.2 chimera, both channels were first subcloned into a pBluescript SK^- vector (EcoRI) in which the XbaI polylinker site had been removed (Klenow). Silent mutations were made in Kv1.2 for the purposes of addition of NsiI and XbaI sites into the equivalent positions to *Shaker*, flanking the S1–S2 linker. After removal of unwanted occurrences of these restriction sites at other locations in the channels (again through silent mutagenesis), the *Shaker* S1–S2 linker was subcloned into Kv1.2, and the A291C mutation was made as described above.

Oocyte preparation and injection

Xenopus frogs were terminally anesthetized by immersion in 2 mg/ml tricaine methanesulphonate (Sigma-Aldrich); unless otherwise stated, all chemicals were purchased from Sigma-Aldrich. Stage V–VI oocytes were isolated, and defolliculation was performed through a combination of collagenase treatment involving mild agitation in 1 mg/ml collagenase type 1a for ∼1 h and manual defolliculation. Between defolliculation and injection, oocytes were incubated for 1–18 h in Barth's solution, which contained 88 mM NaCl, 1 mM KCl, 2.4 mM $NaHCO_3$, 0.82 mM $MgSO_4$, 0.33 mM $Ca(NO_3)_2$, 0.41 mM $CaCl_2$, and 20 mM HEPES, titrated to pH 7.4 using NaOH. Injection of 50 nL cRNA encoding the construct of interest was performed using a Drummond digital microdispensor (Thermo Fisher Scientific) followed by incubation at 19°C in Barth's solution. Currents were recorded 1–4 d after injection. All animal protocols were performed in accordance with University of British Columbia animal care guidelines.

Two-electrode voltage clamp

Oocytes were placed in a bath chamber that was perfused with control ND96 bath solution containing 96 mM NaCl, 3 mM KCl, 1 mM $MgCl_2$, 2 mM $CaCl_2$, and 5 mM HEPES, titrated to pH 7.4 with NaOH. Microelectrodes were filled with 3 M KCl and had resistances of 0.2–2.0 MΩ. Unless otherwise stated, data were recorded from a holding potential of −80 mV. Voltage control and data acquisition were achieved with an amplifier (OC-725C; Warner Instruments) and converter (Digidata 1322 A/D; Axon Instruments) connected to a personal computer running pClamp9 software (MDS Analytical Technologies).

Voltage-clamp fluorimetry

Fluorimetry was performed simultaneously with two-electrode voltage clamp. Labeling of the oocytes with 5 μM TMRM (Invitrogen) dye was performed for 30 min at 10°C in a depolarizing

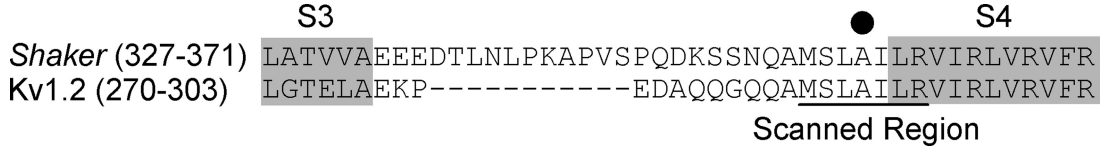

Figure 1. An alignment of the S3–S4 linkers of *Shaker* and Kv1.2 highlights similarities in the region. Gray shading denotes the S3 and S4 regions of the protein. Residues assayed for voltage-dependent fluorescence (Fig. 3) are underlined, and the residue denoted by the closed circle corresponds to Kv1.2 A291C (*Shaker* A359C).

solution containing 98 mM KCl, 1 mM $MgCl_2$, 2 mM $CaCl_2$, and 5 mM HEPES, titrated to pH 7.4 using KOH. Signals were recorded via an inverted microscope (TE300; Nikon) with Epi-Fluorescence attachment and an Electron Tubes photomultiplier tube (PMT; 9124b) module (Cairn Research). TMRM dye, exhibiting maximal light absorption at 542 nm, was excited by light from a 100-W mercury lamp filtered through a 525-nm band pass filter and reflected by a 560-nm dichroic mirror through a 20× objective lens focused on the oocyte. Emitted light, with a maximal emission at 567 nm, was collected by the objective lens and passed through the dichroic mirror to the PMT module. Voltage signals from the PMT were digitized using a converter (Digidata 1322 A/D) and passed to a computer running pClamp9 software to record fluorescence intensity. To minimize fluorophore bleaching, a computer-controlled shutter (Uniblitz; Vincent Associates) was used and opened shortly before application of voltage-clamp pulses. For 100-ms pulses, fluorescence signal sampling frequency was 20 kHz; traces were averaged, with each signal representing the mean of five sweeps, and were filtered offline at 1,000 Hz. To account for any photobleaching of fluorophores that may occur during shutter opening, control fluorescence data were recorded in the absence of any change in voltage and subtracted from the voltage-dependent signal. Fluorescence records were normalized to baseline emission in the absence of a change in voltage to control for cell-to-cell variability, and fluorescence-voltage (*F-V*) relationships are shown normalized to maximum and minimum levels of emission over the voltage ranges tested.

Gating currents

Mammalian tsA201 cells were grown and maintained in MEM at 37°C in an air/5% CO_2 incubator. Media contained 10% bovine serum and 0.5 mg/ml geneticin. On the day before transfection, cells were washed with MEM, treated with trypsin/EGTA for 1 min, and plated on 25-mm^2 coverslips. Wild-type (WT) Kv1.2-pGW1 and green fluorescent protein–pcDNA3 cDNA were then transiently cotransfected using Lipofectamine 2000 (Invitrogen). 24–48 h after transfection, coverslips with adherent cells plated on the surface were placed in a superfusion chamber (volume of 300 µl) containing the control bath solution at room temperature (~25°C). Whole-cell current recording and analysis were performed using an amplifier (Axopatch 200A) and pClamp10 software (Axon Instruments). Patch electrodes were pulled from thin-walled borosilicate glass (World Precision Instruments) on a horizontal micropipette puller (Sutter Instrument Co.). Electrodes had resistances of 1.0–1.5 MΩ when filled with control filling solution. Membrane potentials were not corrected for junction potentials that arose between the pipette and bath solution. Extracellular bath solution contained 140 mM TEA, 10 mM HEPES, 10 mM dextrose, and 1 mM $MgCl_2$, pH adjusted to 7.4 (HCl). Intracellular pipette solution contained 140 mM NMDG, 10 mM HEPES, 1 mM $MgCl_2$, and 10 mM EGTA, pH adjusted to 7.2 (HCl). Cells were maintained at a holding potential of −100 mV, and currents were recorded during 12-ms voltage clamp pulses from −80 to 80 mV in 10-mV increments. Leak subtraction was performed using a −P/6 protocol from holding potential. Data were filtered at 10 kHz and sampled at 100 kHz.

Data analysis

Conductance-voltage (*G-V*) relationships were derived using normalized chord conductance, which was calculated by dividing peak current by the driving force based on the potassium equilibrium potential (internal potassium concentration was assumed to be 99 mM). *F-V* relationships were calculated based on the peak change in emission of the total trace or, in some stated cases, the individual components of the signal. All *G-V*, gating charge-voltage (*Q-V*), and most fluorescence-voltage (*F-V*) relationships were fit with a single Boltzmann function,

$$y = \frac{1}{1+\exp\left[\frac{V_{1/2}-V}{k}\right]},$$

where y is the conductance normalized with respect to the maximal conductance, $V_{1/2}$ is the half-activation potential, V is the test voltage, and k is the slope factor. For analysis of the slow phase of Kv1.2 fluorescence and S289C fluorescence, data were best fit with the following double Boltzmann function:

$$y = \frac{A_1}{1+\exp\left[\frac{(V_{1/2})_1-V}{k_1}\right]} + \frac{A_2}{1+\exp\left[\frac{(V_{1/2})_2-V}{k_2}\right]},$$

where symbols are as described above, A refers to the amplitude of the fit component, and 1 and 2 refer to the separate components of the fit. Unless otherwise indicated, data reported throughout the text and figures are reported as mean ± SEM.

Online supplemental material

Control experiments show that if labeling of the WT Kv1.2 channel at C181 is possible, it does not result in voltage-dependent changes in TMRM fluorescence or interfere with emission from probes attached to residues in other regions of the voltage-sensing domain; this is discussed in the supplemental text. Fig. S1 explores the effect of TMRM on WT Kv1.2 activation and conductance. Fig. S2 compares TMRM fluorescence at A291C in the presence and absence of the removal of the lone potentially labelable endogenous cysteine residue (C181). Fig. S3 shows representative fluorescence traces obtained from a Kv1.5–Kv1.2 chimera channel in which the voltage sensor domain of Kv1.2 was replaced up to and including the S2–S3 linker segment. Fig. S4 shows a structural diagram of the voltage sensor domain, indicating residues in the S1, S2, and S4 regions labeled with TMRM in this study. Online supplemental material is available at http://www.jgp.org/cgi/content/full/jgp.201010413/DC1.

RESULTS

Kv1.2 WT channels do not show voltage-dependent changes in fluorescence emission

Removal of the lone potentially labelable cysteine residue (C181) in the outer S1 greatly reduced channel expression levels, possibly because of a role of this residue in stabilizing interactions between the voltage-sensing and pore domains (Lee et al., 2009). Fig. S1 shows no effects of TMRM on WT Kv1.2 gating and no voltage-dependent changes in emission. Furthermore, fluorescence from a probe attached to A291C shows the voltage-dependent characteristics with and without the WT cysteine at position C181 (Fig. S2). Based on these results, all experiments presented here were performed in the background of Kv1.2 C181 (WT).

Kv1.2 fluorescence at A291C exhibits differences from the *Shaker* A359C homologue

As shown previously (Claydon et al., 2007a), along with activation of ionic currents, TMRM fluorescence from

Shaker C245V A359C shows rapid fluorescence quenching during short depolarizations (Fig. 2, A and B). During large depolarizations, a rapid quenching accounts for 80–90% of the total fluorescence change and correlates with S4 translocation (Mannuzzu et al., 1996; Cha and Bezanilla, 1997, 1998). At potentials negative to activation of ionic current (e.g., −60 mV), fluorescence quenching was still observed, suggesting that some S4 movement precedes pore opening; this is also shown in the comparison of peak *G-V* and *F-V* relationships (Fig. 2 C). In *Shaker* C245V A359C, the $V_{1/2}$ of the *F-V* relationship is left shifted by ∼27 mV compared with the *G-V*.

Kv1.2 A291C ionic current (Fig. 2 D) had similar voltage-dependent and kinetic characteristics to both *Shaker* C245V A359C (Fig. 2 A) and Kv1.2 WT (Fig. S1) channels. In contrast, the fluorophore emissions (Fig. 2, B and E) were strikingly different. Depolarization produced an initial fast fluorescence decay similar to that observed in *Shaker*, which was complete within the first 2–5 ms of depolarization. This was followed by a large secondary slow component that comprised the majority of the total signal and continued for the duration of the depolarization (Fig. 2 E, gray dashed line). Fluorescence quenching was observed at potentials quite negative to channel opening, more so than in *Shaker* (Fig. 2, compare B with E between −80 and −120 mV). Consequently, the total *F-V* relationship was found to be ∼51 mV left shifted compared with the *G-V* (Fig. 2 F), much larger than the left shift in *Shaker* A359C channels (Fig. 2 C).

The slow Kv1.2 fluorescence is recapitulated more or less at other labeled sites in the S3–S4 linker

To investigate whether the differences between Kv1.2 A291C and *Shaker* A359C fluorescence were specific to this position or indicative of a more general difference between the two channels, we performed a scan of seven residues within the S3–S4 linker and S4 in each channel. Three residues N-terminal to A291C (or A359C) and three C-terminal residues (Fig. 1) were tested for voltage-dependent deflections, and typical traces for five of these

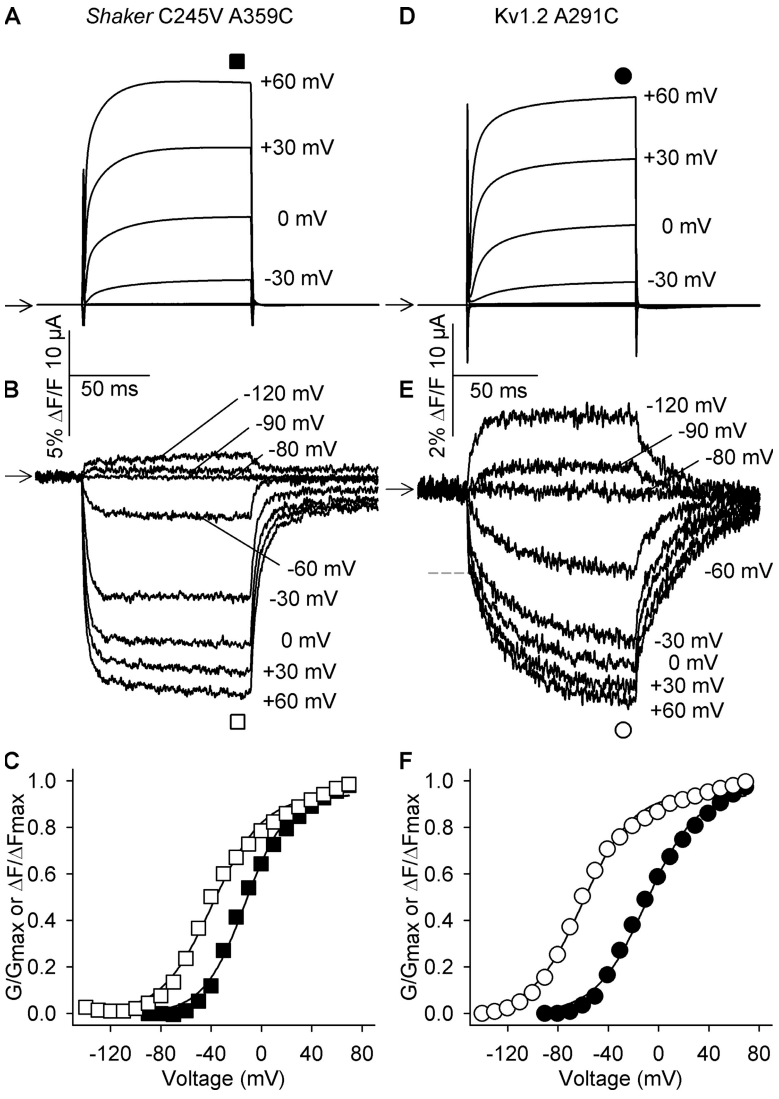

Figure 2. Voltage-dependent *Shaker* and Kv1.2 conductance and fluorescence deflections. Typical current traces (A and D) and fluorescence signals (B and E) are shown for *Shaker* C245V A359C and Kv1.2 C181 A291C for 100-ms pulses between −120 and 60 mV from −80 mV. The dashed line in E marks the approximate division of the two observed components of A291C fluorescence for depolarizations positive to 0 mV. (C and F) Normalized conductance-voltage (*G-V*; closed symbols) and total fluorescence-voltage (*F-V*; open symbols) relationships were calculated from data obtained at the end of each 100-ms pulse (mean ± SEM; n = 7–8), and data were well fit with Boltzmann equations. The $V_{1/2}$ values for *Shaker* C245V A359C were −12.9 ± 1.6 mV and −39.5 ± 1.5 mV for *G-V* and *F-V*, and slope factors (k) were 17.8 ± 1.1 mV and 22.3 ± 1.4 mV, respectively. The Kv1.2 A291C *G-V* had a $V_{1/2}$ and slope factor of −11.2 ± 1.6 mV and 22.4 ± 0.9 mV, respectively, whereas the *F-V* relationship had a $V_{1/2}$ and k of −62.9 ± 1.2 mV and 23.2 ± 1.0 mV.

are shown for *Shaker* (Fig. 3 A) and Kv1.2 (Fig. 3 B) for 100-ms pulses to 60 mV. Previous studies have extensively scanned the externally accessible residues of *Shaker* (Gandhi et al., 2000; Pathak et al., 2007), although these studies have been more concerned with changes occurring on the order of seconds rather than milliseconds. As a result, it is difficult to draw direct comparisons between these data and previous work other than to say the directionality of the changes in fluorescence (quenching vs. dequenching) appear to be the same. We were able to obtain deflections for all seven residues in *Shaker* and six of seven residues in Kv1.2, with the R294C construct not expressing any discernible current or fluorescence in >40 cells attempted. In both *Shaker* C245V L361C and Kv1.2 L293C, we were only able to obtain fluorescence deflections upon hyperpolarization (unpublished data).

Residues in the *Shaker* S3–S4 linker showed a predominantly rapid quenching phase, with a negligible or very small slow quenching component. In Kv1.2, M288C and S289C as well as A291C exhibited a distinct slow quenching phase in addition to the initial fast component. Conductance- and fluorescence-voltage relationships of the first four residues of the scan for both *Shaker* and Kv1.2 are shown in Fig. 3 (C–F). All data are well fit with a single Boltzmann function (Table I), with the exception of Kv1.2 S289C fluorescence, which can be reasonably fit with a double Boltzmann function. The first component of this relationship, scaled to its maximum value at −20 mV, is shown in gray in Fig. 3 D. Overall, the data show that the negative shift in the *F-V* relationship between Kv1.2 and *Shaker* observed with A291C/A359C (Fig. 3 F) is not confined to this residue, as S289C and L290C (Fig. 3, C–E) also show hyperpolarized *F-V* relations compared with *Shaker* equivalent residues. The data suggest that global rearrangements of the Kv1.2 voltage sensor domain occur at more negative potentials relative to observed gating movements in the *Shaker* channel.

Increases in Kv1.2 fluorescence upon hyperpolarization reflect mobility of the voltage sensor

As seen in Fig. 2, there were large differences between *Shaker* and Kv1.2 in the extent of fluorescence change when channels were pulsed to potentials more negative than −80 mV. Depolarizations from −120 mV still showed the same biphasic fluorescence phenotype as that seen from −80 mV, although hyperpolarizations from this voltage no longer resulted in increased fluorescence emission.

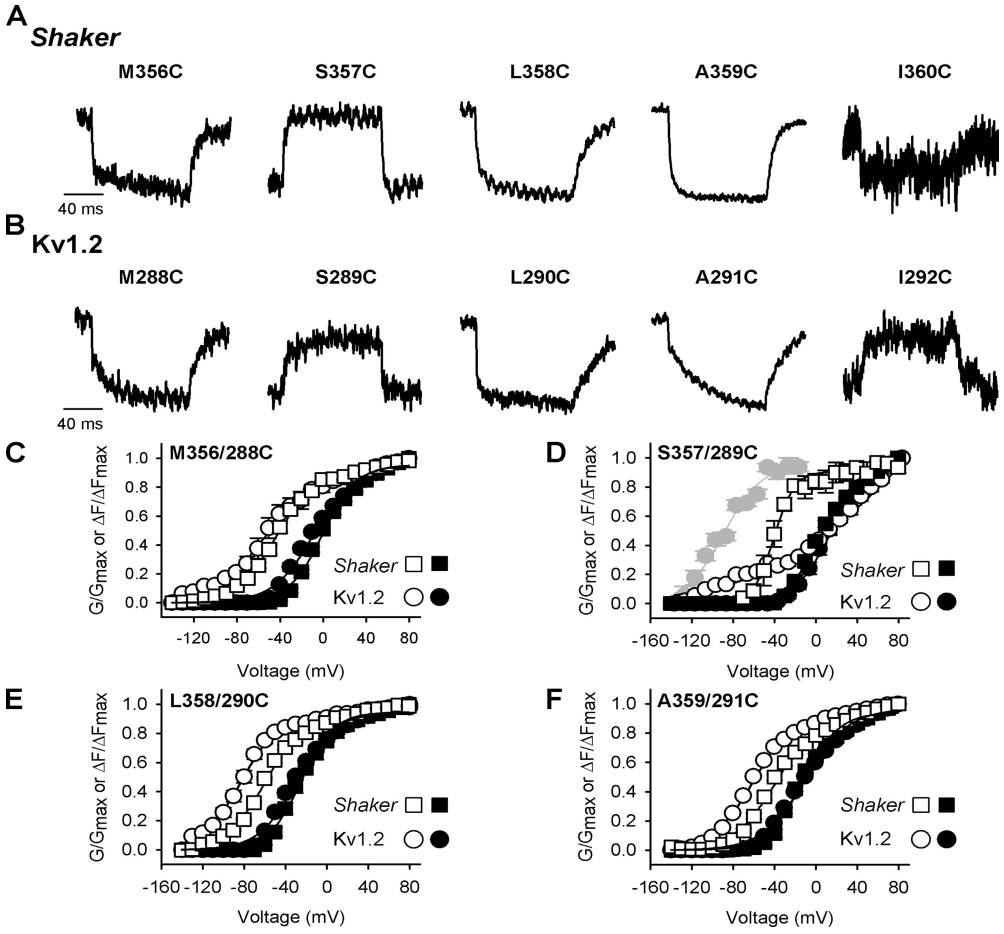

Figure 3. A scan of the *Shaker* and Kv1.2 S3–S4 linkers reveals differences in fluorescence phenotypes. (A and B) Representative fluorescence traces collected in a cysteine scan of five consecutive homologous residues in the S3–S4 linker and N-terminal end of S4 in *Shaker* (A) and Kv1.2 (B). Cells expressing these constructs were held at −80 mV and depolarized to 60 mV for 100 ms. (C–F) Normalized *G-V* (closed symbols) and *F-V* (open symbols) relationships for four of the five *Shaker* (squares) and Kv1.2 (circles) constructs expressing changes in fluorescence upon depolarization, as labeled in the top left corner of each panel. For Kv1.2 S289C (D), the gray circles and accompanying fit denote the Boltzmann fit to the voltage-dependent fluorescence observed between −140 and −20 mV. Mean half-activation and slope data obtained from the fits to all four mutant constructs for each channel can be found in Table I. Data are shown as mean ± SEM and are the mean of three to eight cells collected from each mutant.

TABLE I

Boltzmann fits to Kv1.2 and Shaker G-V and F-V relationships from Fig. 3

Kv1.2					*Shaker*				
Construct	*G-V*		*F-V*		Construct	*G-V*		*F-V*	
	$V_{1/2}$	*k*	$V_{1/2}$	*k*		$V_{1/2}$	*k*	$V_{1/2}$	*k*
	mV	*mV*	*mV*	*mV*		*mV*	*mV*	*mV*	*mV*
M288C	−12.4 ± 1.1	23.0 ± 0.4	−56.9 ± 3.5	26.2 ± 1.6	M356C	−0.5 ± 1.5	17.3 ± 0.7	−41.8 ± 2.6	20.0 ± 1.7
S289C (1)	9.8 ± 3.3	18.1 ± 0.7	−105.0 ± 2.8	−9.3 ± 2.6	S357C	5.6 ± 2.3	18.6 ± 1.1	−42.9 ± 4.4	9.7 ± 1.2
S289C (2)	n/a	n/a	41.7 ± 9.2	−33.3 ± 2.0	–	n/a	n/a	n/a	n/a
L290C	−39.3 ± 4.7	26.5 ± 4.7	−91.9 ± 2.4	19.7 ± 1.7	L358C	−26.2 ± 4.2	18.2 ± 1.8	−59.5 ± 0.5	21.6 ± 1.7
A291C	−12.6 ± 1.9	26.1 ± 1.4	−62.5 ± 1.3	23.3 ± 1.0	A359C	−14.6 ± 1.7	19.8 ± 1.4	−38.8 ± 1.9	22.6 ± 1.4

n/a, not applicable. Mean half-activation ($V_{1/2}$) and slope (*k*) data were calculated from single Boltzmann fits to the data, with the exception of the *F-V* relationship for S289C, which was best fit with a double Boltzmann function.

When cells were held at −50 mV (Fig. 4 B), the fluorescence increase was much greater upon hyperpolarization, and fluorescence observed during depolarization was smaller and composed almost exclusively of a fast quenching component. Ionic currents (unpublished data) and *G-V* relationships (Fig. 4 C, closed symbols) were not any different between the three holding potentials. Furthermore, peak *F-V* relationships were unchanged when total increases in fluorescence emission at hyperpolarized potentials were taken into account (Fig. 4 C, open circles). Peak *F-V* data from a holding potential of −120 mV (Fig. 4 C, squares) and −50 mV (Fig. 4 C, circles) had half-activation voltages of −69.5 ± 2.0 mV and −69.9 ± 5.8 mV, respectively, compared with −69.1 ± 4.5 mV at −80 mV. These data suggest that the fluorescence unquenching at hyperpolarized potentials reflects the holding potential–dependent position of the voltage sensor domain relative to its environment and that mobility of this region reaches one of its extreme positions at or close to −120 mV.

The fact that Kv1.2 *F-V* relationships are similar to holding potentials between −50 and −120 mV also suggests that only readily reversible gating changes occur over this potential range. Although it has been shown that Kv1.2 channels do not undergo significant inactivation of ionic current (Paulmichl et al., 1991; Russell et al., 1994), it is well known that in *Shaker* and other Kv1 channels, prolonged depolarizations associated with inactivation immobilize off-gating charge and shift the *Q-V* relationship in the hyperpolarized direction as a result of stabilization of the S4 segment in an activated conformation and delay its return upon hyperpolarization (Fedida et al., 1996; Chen et al., 1997; Olcese et al., 1997). In *Shaker*, holding the membrane potential at −50 mV resulted in an ∼40-mV hyperpolarizing shift of the A359C *F-V* relationship compared with those from −80 and −120 mV (Fig. 4 D, open squares) despite minimal differences between the corresponding *G-V* relationships. Given that fluorophore labeling at this *Shaker* residue has been shown to track changes in S4 environment during activation, these data suggest impaired movement of the *Shaker* S4 helix at −50 mV compared with −80 and −120 mV, consistent with holding potential–dependent modulation of S4 gating.

The fast and slow fluorescence phases in Kv1.2 have different voltage dependencies

We have shown that upon depolarization, fluorescence from the S3–S4 linker of Kv1.2 A291C shows two distinct phases of quenching: a fast quenching component followed by a slower secondary quenching component that continues for the duration of the depolarization. Fig. 5 A shows a typical fluorescence trace during a depolarization to 60 mV, best fit with a biexponential function (gray dashed line) at this and all other potentials tested. Approximately 40% of the total deflection comprised a fast quenching component with a time constant of ∼1.3 ms, whereas the remaining 60% of quenching occurred ∼20 times slower, with a time constant of 23.9 ms in this particular example. The time constants of the rapid quenching component ($\tau_{F,\,fast}$) increased with depolarization (3.87 ± 0.6 ms at −40 mV compared with 1.2 ± 0.3 ms at 80 mV) and were faster than the ionic current activation time constants at all potentials, whereas the slow quenching component ($\tau_{F,\,slow}$) was clearly slower than activation at depolarized potentials and showed little voltage dependence (Fig. 5 B). These data suggest that the fast fluorescence may report on a process required for activation, whereas the event that the slow fluorescence change reflects is not required itself for channel opening.

As a function of potential, it is clear that each component of the total fluorescence signal is distinct (Fig. 5 C). The slow phase of fluorescence (Fig. 5 C, open squares) was clearly fitted with a double Boltzmann function with widely separated $V_{1/2}$s of −80 and 44 mV. Most (89%) of the slow fluorescence corresponded to a change in voltage sensor environment that occurred at more negative potentials based on the hyperpolarized position of the *F-V* compared with either the fast quenching movement (Fig. 5 C, open circles)

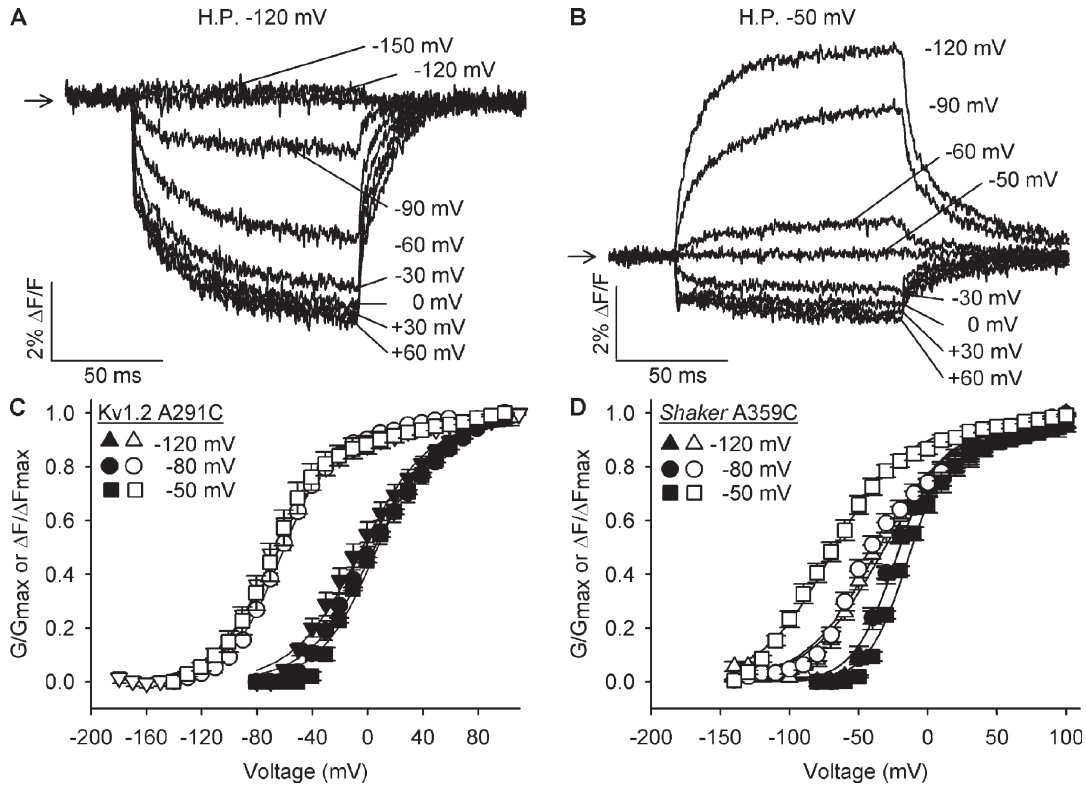

Figure 4. Holding potential affects the directionality of Kv1.2 fluorescence deflections but does not affect the overall *F-V* relationship. (A and B) Representative deflections of Kv1.2 C181 A291C held at −120 (A) and −50 mV (B) in response to 100-ms changes in voltage between −150 and 60 mV. (C) Normalized *G-V* (closed symbols) and total *F-V* (open symbols) relationships for Kv1.2 C181 A291C from three different holding potentials (mean ± SEM; $n = 3–5$), with *F-V* relationships adjusted to account for upward deflections. From −120 mV (triangles), the *G-V* had a $V_{1/2}$ of −10.7 ± 2.5 mV and a slope factor of 24.8 ± 0.9 mV and corresponding values of −69.5 ± 2.0 mV and 22.7 ± 1.1 mV, respectively, for the *F-V*. $V_{1/2}$ and slope factor data from −80 mV (circles) were −2.2 ± 2.3 mV and 24.6 ± 0.7 mV for the *G-V* and −69.1 ± 4.5 mV and 20.8 ± 0.8 mV for the *F-V*. At −50 mV (squares), the $V_{1/2}$ and slope factor for the *G-V* and *F-V* were 2.6 ± 0.8 mV and 24.2 ± 1.1 mV and −69.9 ± 5.8 mV and 22.6 ± 1.5 mV, respectively. (D) *Shaker* A359C *G-V* and *F-V* relationships from the same three holding potentials as in C (mean ± SEM; $n = 7–8$). From −120 mV (triangles), the *G-V* had a $V_{1/2}$ of −22.2 ± 2.1 mV and a slope factor of 15.8 ± 1.6 mV and corresponding values of −35.0 ± 4.5 mV and 27.5 ± 1.6 mV, respectively, for the *F-V*. $V_{1/2}$ and slope factor data from −80 mV (circles) were −22.1 ± 1.9 mV and 15.9 ± 1.7 mV for the *G-V* and −39.8 ± 4.0 mV and 29.1 ± 2.1 mV for the *F-V*. At −50 mV (squares), the $V_{1/2}$ and slope factor for the *G-V* and *F-V* were −12.7 ± 1.9 mV and 15.6 ± 1.7 mV and −79.6 ± 4.8 mV and 32.4 ± 1.5 mV, respectively.

or ionic conductance (Fig. 5 C, closed circles). The second component of this slow fluorescence quenching, present only at very positive potentials, constitutes a relatively minor component (∼10%) of the total slow fluorescence signal, similar to that observed presently (Fig. 2 B) and previously in *Shaker* A359C (Claydon et al., 2007a).

The separation of the fast and slow fluorescence components is well illustrated by comparing fluorescence records from different holding potentials (Fig. 5 D). The fast phase of fluorescence differs only slightly (∼20%) during a pulse to 60 mV from either −80 or −50 mV, whereas the slow component is reduced by more than two thirds. A similar result can be seen during a depolarization to −30 mV from the same two potentials. These data clearly support the idea that the fast and slow components of fluorescence can be modulated separately from one another and thus likely represent different conformational changes within the channel.

The fast phase of fluorescence correlates with S4 movement and the *Q-V* relationship

In *Shaker* A359C, rapid fluorescence quenching upon depolarization has been correlated with the translocation of S4 gating charge, based on the comparison of *F-V* and *Q-V* relationships (Mannuzzu et al., 1996; Cha and Bezanilla, 1997, 1998). Given the speed and voltage dependence of the fast phase of Kv1.2 A291C fluorescence, it seemed appropriate to measure the charge-voltage (*Q-V*) relationship of Kv1.2. However, simultaneous measurement of gating currents with voltage clamp fluorimetry was not possible in the oocyte because of the clamp speed limitations of two-electrode voltage clamp. Therefore, we recorded Kv1.2 gating currents from tsA201 cells using whole-cell patch clamp, as described in the Materials and methods. Fig. 6 A shows representative on-gating currents during 12-ms pulses from a holding potential of −80 mV up to 60 mV. To our knowledge, these are the first reported measurements of Kv1.2 gating currents, and they look

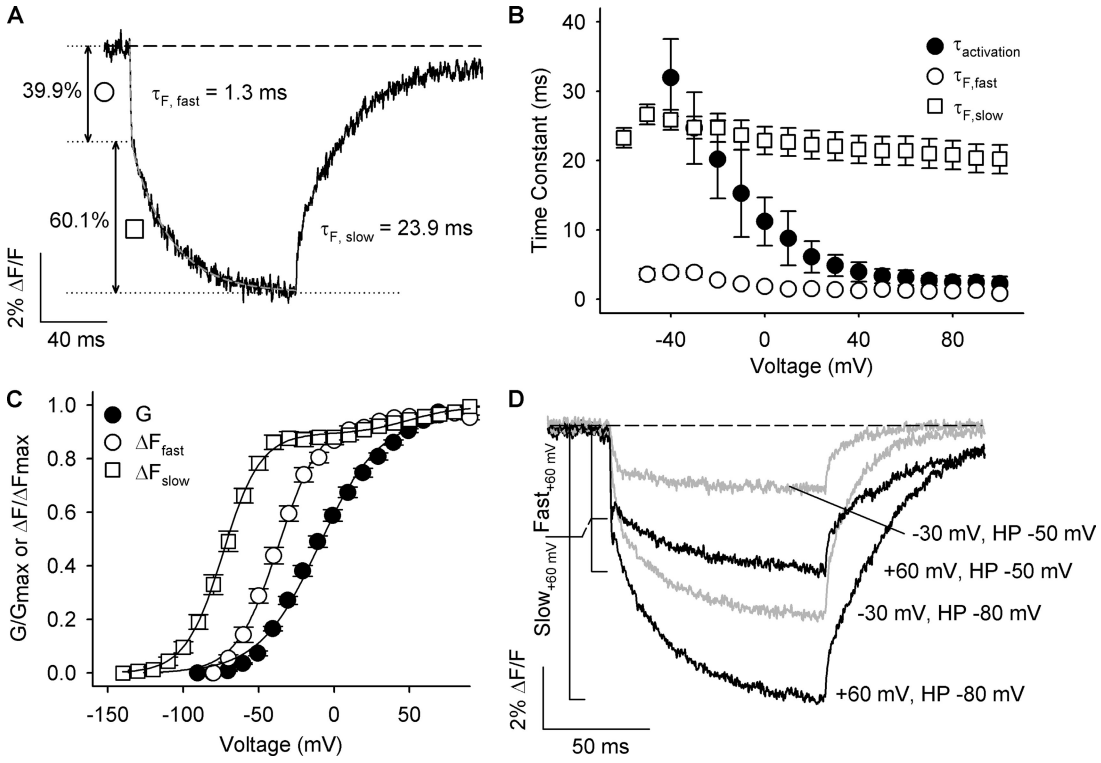

Figure 5. Kv1.2 A291C voltage-dependent fluorescence is well characterized by a double exponential function. (A) Fit of the Kv1.2 A291C fluorescence signal at 60 mV to a double exponential shows that ~40% of the signal amplitude results from a fast movement, with a time constant of 1.3 ms. The slow phase, comprising 60% of the total signal, is slower by an order of magnitude, 23.9 ms in this example. (B) Mean ± SEM time constants of the fast and slow fluorescence signal components (n = 14–20) compared with time constants of ionic current activation fit from ~50% of maximal activation. (C) Normalized *F-V* relationships of the fast and slow components of Kv1.2 A291C fluorescence normalized and plotted alongside the *G-V* relationship (n = 11). The normalized fast phase, fit to a Boltzmann distribution, had a $V_{1/2}$ and slope factor of −39.5 ± 2.0 mV and 15.6 ± 1.0 mV. The voltage dependence of the slow phase was best fit with a double Boltzmann function, with the first component having a $V_{1/2}$ and k of −73.9 ± 1.4 mV and 12.0 ± 0.5 mV (amplitude = 88.7 ± 2.3%) followed by a second component (11.2 ± 2.5%) with respective $V_{1/2}$ and slope factors of 44.3 ± 4.2 mV and 11.6 ± 3.0 mV. (D) Holding potential–dependent separation of the fast and slow fluorescence components. Representative fluorescence traces are shown for Kv1.2 C181 A291C channels depolarized to −30 mV (gray traces) or 60 mV (black traces) from holding potentials (HP) of either −80 or −50 mV as labeled. The two vertical lines to the left of the fluorescence records show the contributions of fast and slow quenching components for depolarizations to 60 mV.

much the same as other Kv1 gating current recordings from mammalian cells (Hesketh and Fedida, 1999). The *Q-V* relationship during depolarization (Fig. 6 B, closed triangles) matched the voltage dependence of the fast fluorescence (Fig. 6 B), and both relationships were well fit with a Boltzmann function, with half-activation voltages of −31.5 ± 2.0 mV and 239.5 ± 2.0 mV for the *Q-V* and fast *F-V* relationships, respectively. The time course of gating charge movement and fast fluorescence quenching is shown for a range of potentials in Fig. 6 C and is reasonably well matched, given the limited time resolution of the oocyte clamp. When the time course of the integrated gating charge movement was fit with a double exponential function, the slow component correlated well with the fast change in fluorescence emission (Fig. 6 D), as has been reported in *Shaker* channels (Cha and Bezanilla, 1997). These data support the idea that a fluorophore attached at the external end of S4 in Kv1.2 reports fast changes in fluorescence emission that correlate with the movement of gating charge and thus S4 movement and channel activation.

Slow changes in fluorescence recovery match the rates of Kv1.2 channel deactivation and reactivation

The major component of slow fluorescence quenching had a voltage dependence that was hyperpolarized from both gating charge movement and pore opening (Fig. 5 C). Given the voltage-dependent and kinetic properties of the fluorescence change, it is unlikely that the slow phase can be associated with pore opening. However, we did find that the time course of slow fluorescence recovery after repolarization was strongly correlated with both channel deactivation and also reavailability after progressively longer interpulse intervals, as illustrated in Fig. 7. After depolarizations to a range of potentials, fluorescence increased back to baseline with an identical time course to the deactivation of ionic current at −120 mV (Fig. 7 A) or a range of potentials

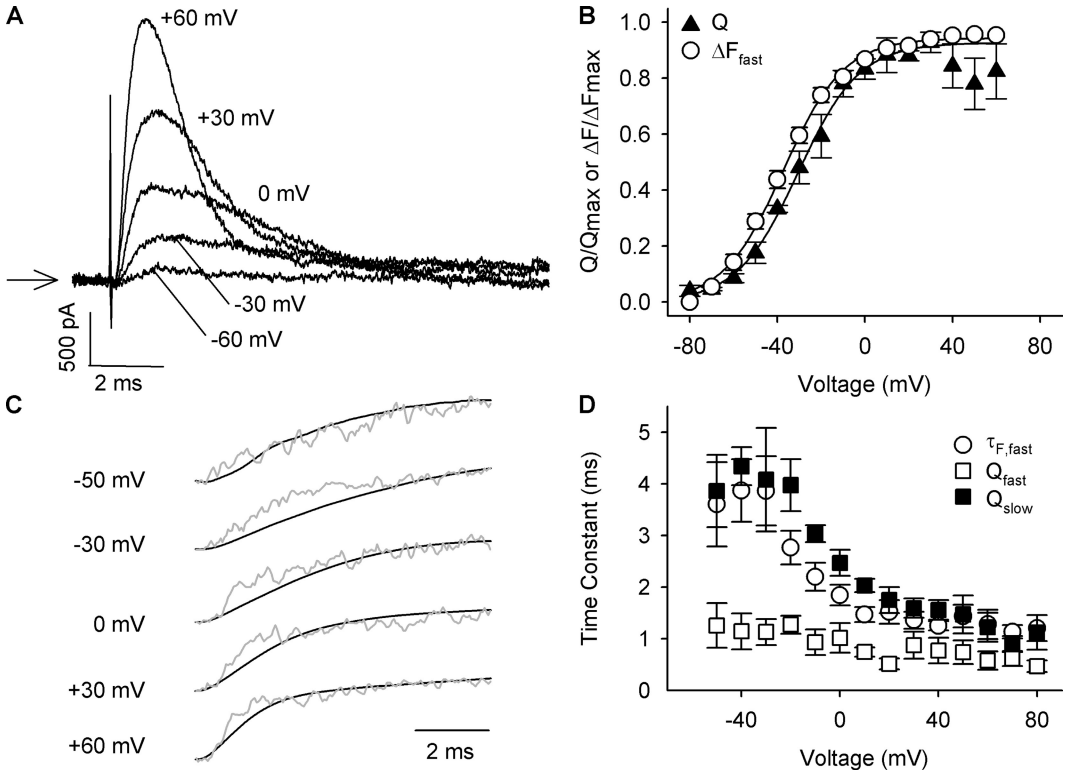

Figure 6. Correlation of the fast component of Kv1.2 fluorescence quenching with gating charge movement. (A) Representative gating currents for Kv1.2 WT, recorded from transiently transfected tsA201 cells. Data were recorded from 12-ms pulses from −80 to 60 mV at 10-mV increments; only every third voltage is shown here for clarity. (B) Overlay of the mean normalized charge-voltage (*Q-V*) relationship with the fast *F-V* relationship from Fig. 5 C. The *Q-V* relationship $V_{1/2}$ and *k* values were −31.5 ± 2.0 mV and 11.5 ± 0.6 mV, respectively. (C) Superposition of fluorescence (gray) and cumulative gating charge (black) versus time in Kv1.2 channels. Data are shown for a range of depolarizations from −50 to 60 mV, as labeled, for the initial 8 ms of depolarization in the case of the fluorescence data and are normalized to the respective maximum values. The fluorescence quenching at this potential is inverted to more closely compare with the gating charge data. (D) Mean time constants of the integrated gating charge movement compared with the fast fluorescence quenching of A291C. Gating charge data were fit to a double exponential function, and the mean ± SEM data (n = 10–15) of the fast (closed squares) and slow (open squares) components were plotted as a function of voltage. Time constants for the fast quenching event (open circles) are as plotted in Fig. 5 B.

(Fig. 7, B and C). For example, deactivation of ionic current to −120 mV occurred with a mean time constant of 7.6 ± 1.5 ms, similar to that observed in previous studies (Watanabe et al., 2007; Lewis et al., 2008), compared with a time constant of 9.3 ± 0.5 ms for the change of fluorescence emission.

The reactivation of Kv1.2 channels during a two-pulse protocol is shown in Fig. 7 D. After short P1–P2 intervals (e.g., 6.25 ms) at −80 mV, the slow fluorescence quenching during the P2 pulse to 60 mV was quite small, as expected given that little recovery of the tail had occurred in the interpulse interval. This was accompanied by faster activating ionic currents and greater instantaneous current after a 6.25- or 25-ms P1–P2 interval. A scaled and inverted fit of the slow off-fluorescence (Fig. 7 D, gray dashed line) matched the recovery of the initial ionic current back to P1 values (Fig. 7 D, gray arrow). Fig. 7 E shows mean data for the normalized instantaneous current in the P2 pulse compared with the slow fluorescence recovery after the first P1 pulse. The current reactivation (τ_{ionic} = 15.7 ± 1.3 ms) correlated extremely well with the time dependence of fluorescence recovery (τ_{Fl} = 18.5 ± 0.6 ms), suggesting that the slow fluorescence may track a conformational change in the protein that, upon repolarization, is rate limiting for deactivation of ionic current.

Slow changes in fluorescence emission reflect internal rearrangement within the voltage sensor domain

To investigate whether internal rearrangement within the voltage sensor could explain the slow quenching, we replaced portions of the voltage-sensing domain of Kv1.2 with that from another mammalian *Shaker* homologue, Kv1.5. The fluorescence of Kv1.5 has been characterized in previous studies (Vaid et al., 2008, 2009) and, importantly, does not have a Kv1.2-like slow quenching component in its voltage-dependent fluorescence. We made two chimeras in which Kv1.2 was replaced with Kv1.5 sequence up to the S1–S2 linker (Kv1.5-S12L-Kv1.2) and up to the S2–S3 linker (Kv1.5-S23L-Kv1.2) in the background of A291C (Fig. 8 A). Typical fluorescence records for Kv1.5-S12L-Kv1.2 are shown in Fig. 8 B.

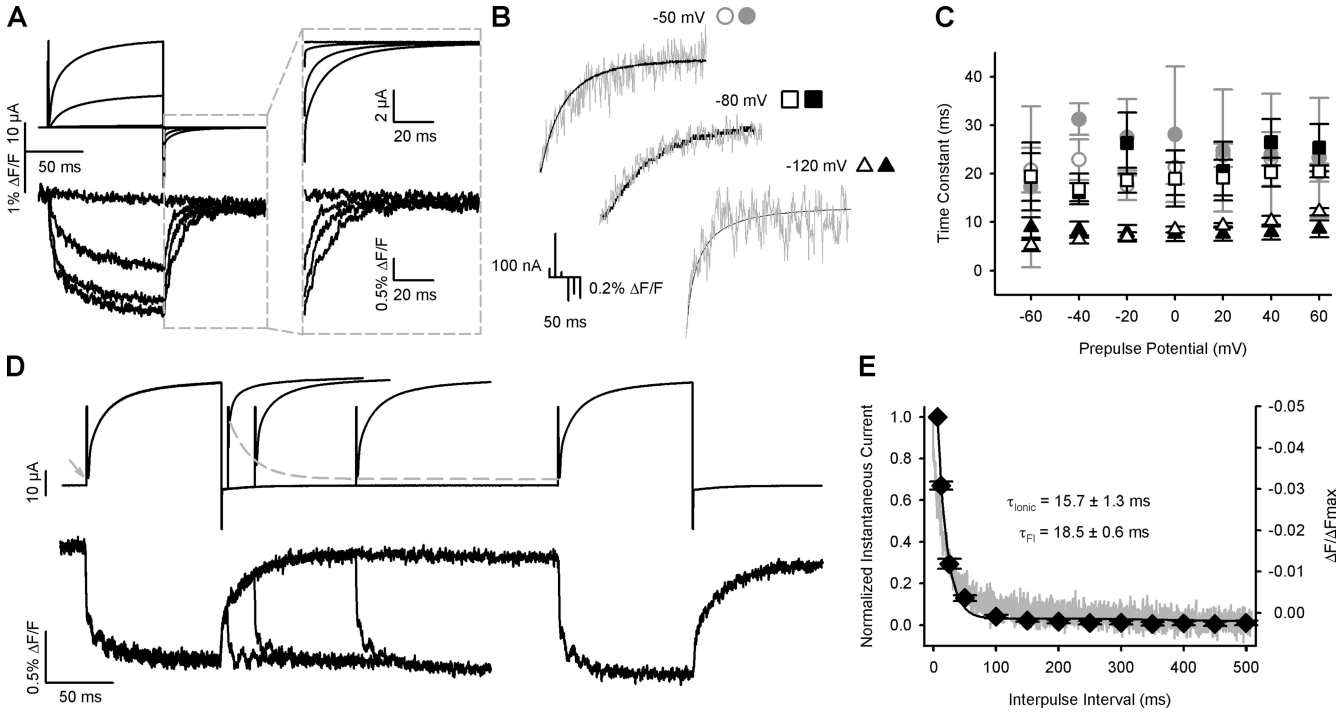

Figure 7. Slow fluorescence return upon hyperpolarization correlates with deactivation of ionic current. (A) Kv1.2 A291C currents (top) and fluorescence (bottom) traces at −120, −60, 0, and 60 mV from a holding potential of −120 mV. The right panels show an enlarged view of the tail currents and off-fluorescence emissions. (B) Overlay of ionic tail current (black lines) and slow off-fluorescence quenching (gray) for Kv1.2 A291C at the three potentials labeled after a depolarization to 20 mV. Scale bars are as shown, left to right, for the corresponding holding potentials. (C) Deactivation and slow off-fluorescence time constants for Kv1.2 A291C at the three holding potentials shown in B as a function of prepulse potential ($n = 3$–5). Mean data are shown every 20 mV for clarity. (D) Representative current and fluorescence records from a dual pulse (P1–P2) protocol with varying interpulse recovery time. Data are shown for 100-ms pulses from −80 to 60 mV with interpulse intervals of 6.25, 25, 100, and 250 ms. For clarity, data are only shown up to the end of the second depolarizing pulse of intermediate records. The gray arrow shows the instantaneous level of ionic current at P1; the gray dashed line is an inverted fit of the slow component of off-fluorescence from P1. (E) Overlay of the slow off-fluorescence component in D with the normalized initial P2 current amplitudes (black diamonds). The black line is a single exponential fit to the ionic current data. Mean time constants for the fits to individual datasets and the off-fluorescence component are shown in the panel ($n = 5$).

Ionic currents during depolarization were unchanged in the chimeric channels (not depicted), but there were marked differences in quenching observed compared with Kv1.2 A291C (Fig. 2 E).

Replacing the first transmembrane segment, S1, and the extracellular S1–S2 linker with those from Kv1.5 dramatically reduced the slow quenching associated with Kv1.2 A291C fluorescence (Fig. 8 C). The more extensive replacement of the Kv1.2 voltage sensor with the S2 segment and intracellular S2–S3 linker did not have any further effects on the fluorescence (Fig. S3). The fast fluorescence quenching from these channels comprised ∼80% of the total amplitude (similar to *Shaker* A359C over the same time course) compared with only 40% in Kv1.2 A291C. Fluorescence recorded from both chimera channels looked very similar to fluorescence recorded from Kv1.2 A291C from a holding potential of −50 mV (Fig. 4 B), a potential at which the majority of slow fluorescence change had already occurred (Fig. 5 C). A parallel loss of the slow fluorescence recovery on repolarization was observed (Fig. 8, B and C; also see Fig. S3), and, importantly, the S12L chimera showed accelerated ionic current deactivation that matched the time course of fluorescence decay (Fig. 8 C, inset), further suggesting that these two processes are linked through some common or related molecular rearrangement.

In the *F-V* relationships, the lack of a slow component of fluorescence at hyperpolarized potentials in the two Kv1.5–Kv1.2 constructs resulted in a depolarizing shift of the *F-V* relationship (Fig. 8 D), with no change in the *G-V*. The fast fluorescence quenching, with time constants on the order of milliseconds, showed an identical voltage dependence to the fast component of Kv1.2 A291C (Fig. 8 E, circles) and the Kv1.2 *Q-V* relationship (Fig. 8 F), suggesting that the majority of the remaining fluorophore quenching in the chimera reports conformational changes associated with S4 translocation. The residual slow component of fluorescence in the chimera evident at more depolarized potentials had a $V_{1/2}$ of 33.4 ± 2.5 mV (unpublished data), which is very similar to the small slow component of WT Kv1.2 fluorescence.

A third chimera channel in which only the S1–S2 linker of Kv1.2 was replaced with the equivalent segment from *Shaker* (Fig. 9 A) resulted in the complete abolition

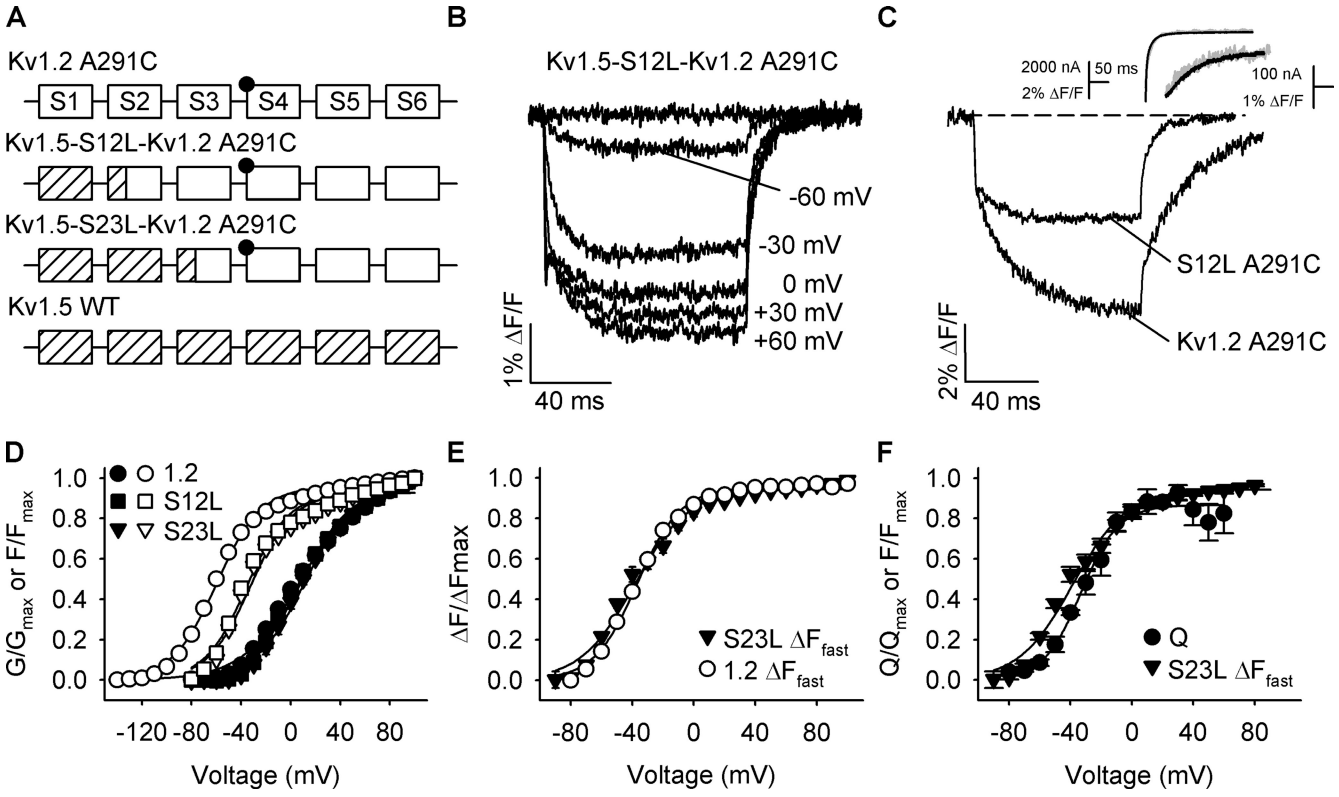

Figure 8. Kv1.2–Kv1.5 chimera channels lack the slow fluorescence quenching at negative potentials. (A) Cartoon representation of Kv1.2 A291C (top), Kv1.5 WT (bottom), and the two chimeric channels (middle cartoons). Open squares (and their connecting segments) originate from Kv1.2, and slashed squares are Kv1.5 segments. A291C is located approximately with closed circles at the N-terminal S4. (B) Representative fluorescence traces from the Kv1.5-S12L-Kv1.2 A291C chimera. Data were collected using the protocol outlined in Fig. 2. (C) Overlay of representative fluorescence deflections for Kv1.2 A291C and Kv1.5-S12L-Kv1.2 (S12L) A291C for depolarizations to 30 mV normalized to the fast fluorescence quenching components. The inset shows overlays of deactivating ionic tail currents and off-fluorescence of Kv1.5-S1S2L-Kv1.2 A291C (top) and Kv1.2 A291C (bottom), with scale bars as noted. (D) Mean normalized *G-V* (closed symbols) and *F-V* (open symbols) relationships for the Kv1.5/Kv1.2 chimera channels compared with Kv1.2 A291C, shown ±SEM ($n = 10–13$). Boltzmann fits to the data from Kv1.5-S12L-Kv1.2 A291C (S12L) gave $V_{1/2}$ and k values of 2.6 ± 2.6 mV and 23.9 ± 0.9 mV and −40.3 ± 3.1 mV and 28.4 ± 2.6 mV for *G-V* and *F-V*, respectively; the fits to Kv1.5-S23L-Kv1.2 A291C (S23L) were 7.3 ± 1.9 mV and 23.9 ± 0.7 mV for the *G-V* relationships and −40.9 ± 2.2 mV and 23.4 ± 2.3 mV for the *F-V* relationships. Kv1.2 A291C values are as reported in Fig. 4. (E) Voltage-dependence plots of the fast fluorescence component of Kv1.5-S23L-Kv1.2 A291C with that of Kv1.2 A291C from Fig. 5 C. $V_{1/2}$ and k values were −40.3 ± 2.2 mV and 19.5 ± 1.7 mV for the chimera channel ($n = 15–17$). (F) Mean normalized *F-V* relationship of the fast component of Kv1.5-S23L-Kv1.2 A291C emission, overlaid with the Kv1.2 *Q-V* relationship (closed circles) from Fig. 6 B.

of slow fluorescence from A291C, similar to the Kv1.5–Kv1.2 chimeric channels (Fig. 9 B), whereas ionic currents were unchanged (not depicted). The loss of fluorescence is particularly apparent at negative potentials between −120 and −50 mV where the slow phase of Kv1.2 was most prominent and highlights the importance of the linker region in detecting slow reorganizations of the voltage sensor.

The S1–S2 linker and S4 region are both intricately involved in Kv1.2 activation

The ability of a TMRM fluorophore attached to residue C291 to report on movements of both S4 and the S1–S2 region suggested to us that these two regions are sufficiently close in one or both of the closed and open states to alter the S4 fluorophore environment in a voltage-dependent manner. To test whether S1–S2 movements alone were responsible for slow changes in Kv1.2 fluorescence, we recorded voltage-dependent fluorescence directly from cysteines inserted in the S1–S2 linker (Fig. 10 A, boxed residues), which, based on the crystal structure, are somewhat more distant from S4 and the pore region compared with A291C in the S3–S4 linker (Fig. 11). Test residues were located near the outer end of S1 (I187) or S2 (F218, T219, and D220) as well as in the middle of the linker, positioned toward adjacent subunits in the crystal structure (S208 and T209; Long et al., 2005b). Of these, only two constructs gave voltage-dependent deflections: I187C (Fig. 10 B) and T219C (Fig. 10 C; shown in bold in the alignment in Fig. 10 A), and both showed only slow quenching.

Labeled I187C channels showed slow voltage-dependent emission quenching with time constants similar to the slow fluorescence emission from Kv1.2 A291C (Fig. 5)

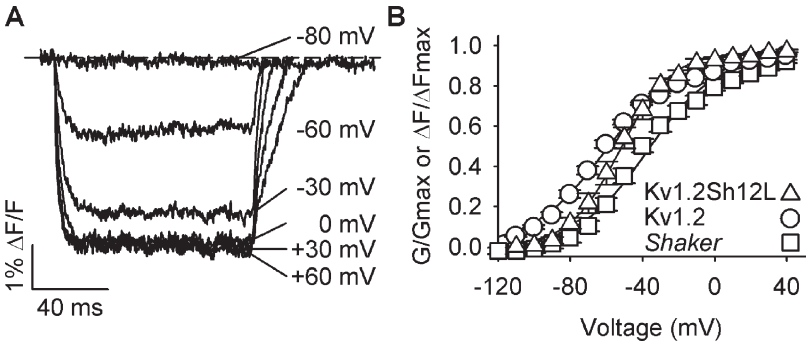

Figure 9. Effect of *Shaker* S1–S2 linker replacement on Kv1.2 fluorescence. (A) Representative fluorescence records from a Kv1.2-*Shaker* S1–S2 linker A291C chimera channel (Kv1.2Sh12L). Traces are shown for depolarizations to potentials as labeled, using the same protocol as outlined in Fig. 2. (B) Mean *F-V* relationship for Kv1.2Sh12L (triangles) compared with Kv1.2 A291C (circles) and *Shaker* A359C (squares) as previously shown in Fig. 2. For Kv1.2Sh12L, $V_{1/2}$ and k values for the Boltzmann fit were −56.0 ± 2.5 mV and 15.5 ± 0.8 mV (n = 7).

and lacked any evidence of fast fluorescence quenching. The S2 fluorophore T219C also showed only slow decreases in fluorescence emission during depolarizations of a similar time course; this is the homologous residue to T276C in *Shaker*, which has previously been shown to exhibit voltage-dependent fluorescence emission left shifted relative to *Q-V* (Cha and Bezanilla, 1997). In addition, the total *F-V* relationship for T219C fluorescence (Fig. 10 D, open triangles) correlated well with the voltage dependence of the slow fluorescence component of A291C and had a similar half-activation potential (−70.8 ± 5.9 mV; Fig. 10 D). I187C did detect movement between −140 and −90 mV, which is clearly apparent in Fig. 10 D, but most changes of fluorescence occurred at more positive potentials.

DISCUSSION

Kv1.2 A291C rapid fluorescence quenching reports fast S4 displacement during channel activation

In Kv1.2, it is only the fluorophores attached to cysteines placed at A291, L290, and M288 at the top of S4 and in the S3–S4 linker that detect rapid quenching as

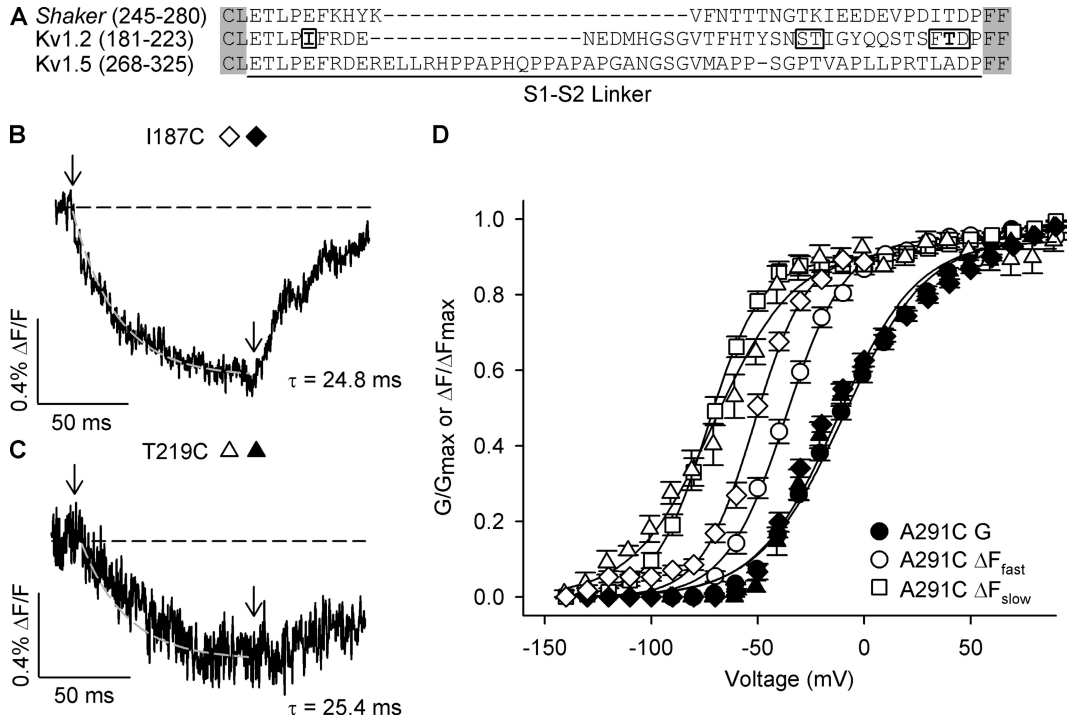

Figure 10. TMRM attached to residues in the S1–S2 linker of Kv1.2 report only slow changes in fluorescence emission in response to voltage. (A) An alignment of best fit for the amino acid residues of the S1–S2 linker region (underlined) of *Shaker*, Kv1.2 and Kv1.5. Residues in gray correspond to portions of the S1 and S2 helices. Residues tested for fluorescence are boxed, and those giving voltage-dependent deflections are in bold. (B and C) Representative fluorescence emissions recorded at 60 mV from I187C (B) and T219C (C) channels. (D) Mean *G-V* (closed symbols) and *F-V* (open symbols) relationships for I187C (diamonds) and T219C (triangles; n = 6–15) compared with Kv1.2 A291C fast and slow fluorescence components from Fig. 5 C (open circles and squares, respectively). Boltzmann fits to I187C data gave $V_{1/2}$ and k values of −50.6 ± 1.4 mV and 10.6 ± 0.5 mV for *F-V* and −17.7 ± 1.9 mV and 27.3 ± 1.0 mV for *G-V*. T219C half-activation potential and slope factor values were −15.5 ± 2.6 mV and 22.8 ± 0.3 mV and −70.8 ± 5.9 mV and 18.3 ± 2.0 mV for the *G-V* and *F-V* relationships. Error bars represent mean ± SEM.

part of the overall fluorescence signal during depolarization (Fig. 3 B). From closed and open state models of Kv1.2 (Fig. 11 and Fig. S4), the positions of these amino acids suggest that rapid quenching is best detected by residues at the top of S4 that face either S5 (of the adjacent subunit) or the voltage sensor domain in the closed state, likely as a result of the positioning of the fluorescent probe in an environment subject to significant voltage-dependent change. In contrast, residues that face away from protein, S289 and I292, and fluorophores attached to sites deeper in S4 gave only smaller slow signals or no signal at all, which suggested more limited changes in environment during depolarization.

The similarity of the fluorescence reports from probes attached to neighboring residues as well as the periodicity in the appearance of the rapid quenching component support some degree of secondary structure in the S3–S4 linker, in accordance with data from an alanine scan of these residues (Li-Smerin et al., 2000; Li-Smerin and Swartz, 2001). The Kv1.2 crystal structure data are unresolved within the linker regions (Long et al., 2005a,b), but in the Kv1.2/Kv2.1 paddle chimera open state structure (Long et al., 2007) there does appear to be some secondary structure. The rapid quenching observed in Kv1.2 could report one of two possible conformational changes. It could indicate an outward movement of S4, bringing the TMRM probe into a more hydrophilic environment or altering its orientation with respect to nearby quenching amino acids. Alternatively, it could report a rotation of the S4 that, as far as the probe and its environment is concerned, leads to a rapid quenching of TMRM fluorescence. Likely, it is some combination of both, as the open state model of Kv1.2 (Fig. 11, B and D) places the A291C residue in an extruded rotated position, away from the external cavity occupied in the resting state. Recent structural studies have questioned the extent to which this extrusion away from the pore accurately reflects the open state of Kv1.2 (Jogini and Roux, 2007; Lewis et al., 2008), but even a more conservative deviation of S4 away from the pore would support these findings.

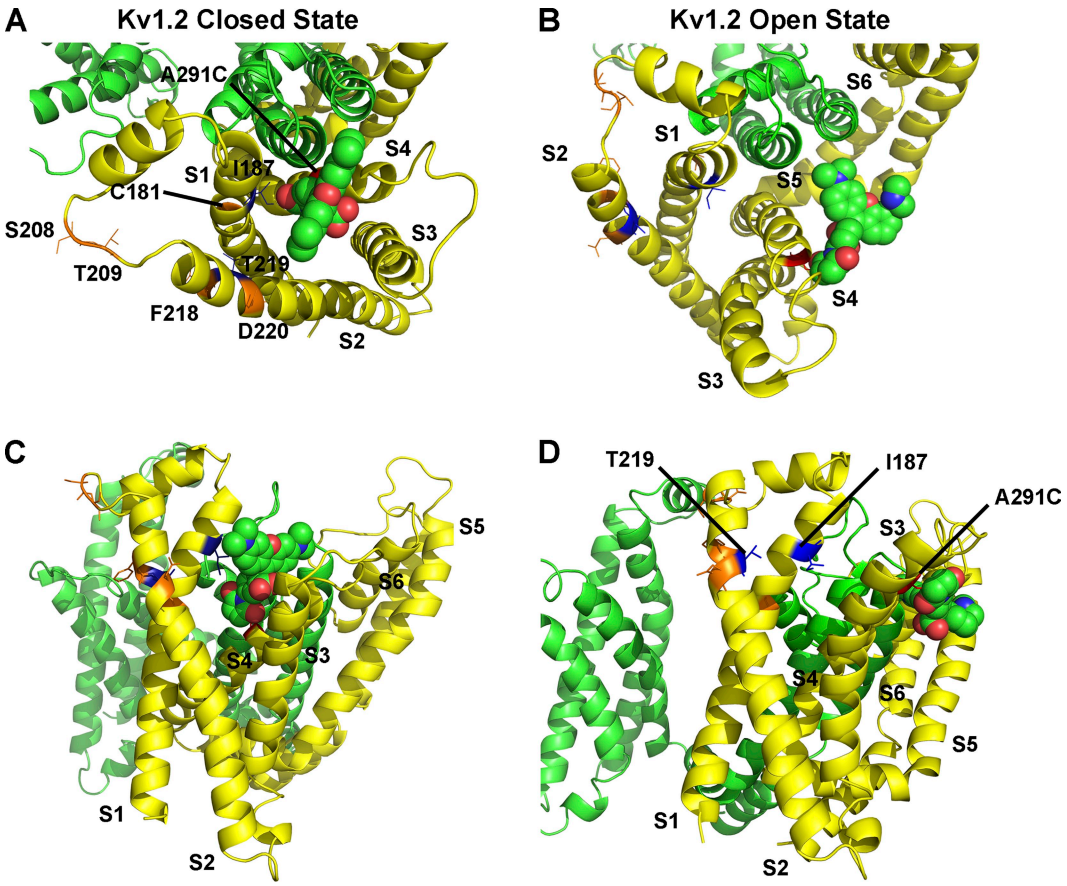

Figure 11. Proposed model of Kv1.2 activation based on TMRM fluorescence. (A) Closed state structure of Kv1.2 A291C-TMRM based on the closed state model of Pathak et al. (2007), shown from the top. Only one voltage-sensing domain (yellow) and the pore domain from an adjacent subunit (green) are shown. Residues tested are labeled and highlighted based on their ability (blue) or inability (orange) to yield voltage-dependent fluorescence; the A291C mutation is shown in red. The TMRM molecule is modeled within the external aqueous vestibule between S4 and S1–S3 as a spherical structure of carbon (green), oxygen (red), and nitrogen (blue) atoms. (B) Open state structure of Kv1.2 A291C-TMRM. The view shown, looking down on the channel, is similar to that in A for the closed state channel relative to the pore domain, in particular S5. (C and D) Side views of the closed and open state structures of Kv1.2 A291C-TMRM seen in A and B. Transmembrane helices of one subunit are as labeled in each panel.

In *Shaker*, the mainly fast fluorescence emission has been shown to have a voltage dependence similar to (Cha and Bezanilla, 1997) or identical (Mannuzzu et al., 1996) to that of the *Q-V* relationship. Here, in the first published recordings of Kv1.2 gating currents, we also observed a strong correlation between the voltage dependencies of fast fluorescence quenching and gating current measurements (Fig. 6 B). Small differences in the time course and voltage dependence of gating charge movement and fluorescence quenching may reflect imperfect separation of the fast and slow components of fluorescence or simply methodological differences between mammalian and oocyte cellular models. It should be noted that the probe is also reporting on local changes in S4, whereas other regions of the voltage sensor, in particular S2 and S3, contain charged amino acids that may respond to changes in membrane potential (Seoh et al., 1996) and would be accounted for in a gating charge measurement, but to a lesser degree or not at all in the fluorescence signal from S4 residues.

The fast quenching Kv1.2 A291C signals from both of the Kv1.5–Kv1.2 chimeric channels also resulted in *F-V* relationships identical to the *Q-V* (Fig. 8 F), and, interestingly, when the *Shaker* S1–S2 linker (seven amino acids shorter than Kv1.2) was inserted, the resulting fluorescence (Fig. 9 A) was monophasic. From the rapid fluorescence quenching seen in all constructs by A291C-TMRM, we can conclude that a rapid S4 movement occurs in Kv1.2 that is responsible for the appearance of gating charge, and which eventually leads to channel opening.

Kv1.2 A291C fluorescence also reports slower voltage-dependent rearrangements of the voltage sensor domains

A major novel finding in this work is the description of a prominent voltage-dependent slow phase of fluorescence quenching that originates from movements of the S1–S3 voltage sensor domains of Kv1.2 and that has not been described in prior studies of *Shaker* or Kv1 channels (Mannuzzu et al., 1996; Cha and Bezanilla, 1997; Claydon et al., 2007a; Vaid et al., 2008). In *Shaker*, small slow changes in fluorescence at depolarized potentials were correlated to events in the pore underlying P/C-type inactivation (Loots and Isacoff, 1998, 2000), whereas such changes in Kv1.5 A397C fluorescence were linked to changes in pore structure at the level of the selectivity filter (Vaid et al., 2008). Both Kv1.2 and Kv1.5–Kv1.2 chimera channels (Fig. 8) retain a small slow quenching component at depolarized potentials, suggesting that a similar conformational change may occur in Kv1.2 in the absence of an observable inactivation process. However, none of these channels exhibited such a large slow fluorescence as Kv1.2, nor with such a negative voltage dependence.

The experiments presented here suggest that reversal of these slow movements is obligatory for channel deactivation (Figs. 7 and 8). They may be coupled to the same molecular movements, or the reoriented voltage-sensing domain may interact with either the activated pore or S4, preventing or altering the time course of channel closure. We cannot be sure if the slow reorientation leads to a stabilized activated/open state at positive potentials once the movement is complete because we have not performed experiments to investigate open state stability directly. However, this slow reorientation process of the voltage sensor is reminiscent of S4 entry into a relaxed state, as determined by Villalba-Galea et al. (2008) in *Ciona intestinalis* voltage sensor–containing phosphatase. In their model of activation gating, the activated state of S4 was short lived before entry to this state, although this change in state did not appear to affect the activated state of the effector portion of the protein (i.e., the coupled enzyme or pore moiety).

The S1–S2 linker of Kv1.2 is required for the slow quenching observed in A291C, as substitution of this region with that of Kv1.5 or *Shaker* was sufficient to either abolish or prevent detection of this slow fluorescence change (Figs. 8 and 9). The findings point to an integrated action of the S1–S4 elements of the voltage sensor during channel function, and there is plenty of evidence in the literature to suggest that disruption of S1 or the S1–S2 linker function alters activation gating. In Kv7.1 channels, the S1 helix has been suggested to help "steer" S4 motion through interactions occurring during gating (Haitin et al., 2008), and cross-linking S1 to the pore domain through cysteine–cysteine interactions has also been shown to interfere with the function of KvAP channels, suggesting that some motion of this region may occur (Lee et al., 2009). Localized interactions within the S1–S2 linker have also been shown to modulate channel activation. In chimeric Kv2.1 channels in which the S1–S2 linker was replaced with that from Kv1.2, there was a 34-mV leftward shift in the *G-V* relationship and a two- to threefold decrease in the time constants for activation, suggesting that the S1–S2 region was important in channel stability and capable of modulating gating (Koopmann et al., 2001).

Structurally, the S1–S2 linker of Kv1.2 channels has been suggested to form a coiled loop structure near the external surface of the membrane (Zhu et al., 2003), suggesting flexibility in this region. Differences in the primary sequence of this region between Kv1.2 and *Shaker* or Kv1.5 (Fig. 10 A) and the S3–S4 linker (Fig. 1) could have large effects on the positioning of this flexible segment. In Kv1.2, this may contribute to the positioning of this region with respect to the A291C S4 microenvironment. Additionally, all three channels possess extracellular glycosylation sites in the S1–S2 linker, at a similar position in the linker, although their positioning with respect to the transmembrane helices may differ based on the number of amino acids on either side of the glycosylation site (Fig. 10 A; Zhu et al., 2003). Kv1.2 glycosylation has been shown to modulate Kv1.2 activation gating

(Watanabe et al., 2007), and so may interact with the voltage sensor through positioning of the S1–S2 linker in a manner different than other Kv1 channels.

Slow voltage-dependent rearrangement of the voltage sensor domains is confirmed by fluorophores placed in S1–S2

The fluorophores attached at I187 or T219, which would be likely to occupy a different microenvironment than at A291C, do not detect rapid movement associated with S4 displacement, but the slow movement within S1–S3 seen by A291C-TMRM can be detected by TMRM attached within the S1–S2 region (Fig. 10). Fluorescence quenching at these residues accurately tracks the time course of slow movement of the voltage sensor, whereas the voltage-dependent fluorescence change of T219-TMRM overlays exactly the slow component of A291C-TMRM (Fig. 10 D). The more faithful recapitulation of the voltage dependence of slow fluorescence from T219C compared with I187C may be in part caused by the fact that fluorophores in S2 or S4 are closer to the edge of the protein and therefore experience more significant environmental changes than a fluorophore within S1. Alternatively, the slow movement could be more prevalent within the S2 helix than in S1.

Interestingly, the fluorescence recorded from the homologous T276C residue in *Shaker* (Cha and Bezanilla, 1997) exhibits a considerably faster quenching component and a somewhat smaller leftward shift relative to the *Q-V* relationship (~20 mV). Cha and Bezanilla (1997) suggested that the S2 helix may undergo voltage-dependent movement before S4, facilitating S4 activation but carrying only a small amount of gating charge. However, in Kv1.2, the much slower time course of S1–S3 rearrangement suggests that the motion cannot precede or constrain S4 movement, and indeed it continues well beyond the time required for full channel activation (Fig. 2). Although S2 does contain negatively charged side chains that appear to help stabilize S4 in the resting and activated states (Seoh et al., 1996; Long et al., 2005b, 2007), the minimal voltage dependence of the S1–S3 rearrangement based on time constant data (Fig. 5 B) suggests that little net charge movement within the electric field occurs, and given the extended time course of this rearrangement, it is not surprising that we were unable to resolve any associated gating charge movements.

The data from TMRM attached to A291C suggest that the most extreme inward limit of voltage-dependent movement occurs at approximately −120 mV (Fig. 4). We also conclude that the voltage sensor domain movement, measured as a change in S3–S4 linker environment and S1–S2 rearrangements, is freely reversible between –120 and –50 mV (Fig. 4 C) or that any holding potential–dependent effects on mobility have reversed within 100 ms of return to more negative potentials. This is in agreement with previous work that has characterized the voltage sensor as a fluid portion of the protein (Larsson et al., 1996; Yusaf et al., 1996; Baker et al., 1998; Wang et al., 1999) but different from functional studies in *Shaker* channels in which prolonged depolarization leads to a hyperpolarization of the returning *Q-V* relationship (Olcese et al., 1997). This hyperpolarization is recapitulated in the *Shaker* A359C fluorescence report of S4 movement (Fig. 4 D) but was not seen in Kv1.2. This may reflect the inclusion of rearrangements involving the entire voltage-sensing domain in the Kv1.2 fluorescence record and not just the S4 translocation measured by the rapid initial quenching.

Conclusion

This paper represents the first study of the Kv1.2 voltage sensor domain using fluorimetry and gating currents and highlights at least two independent conformational changes in this region in response to depolarization. A prominent fast change in fluorescence emission at depolarized potentials correlates well with channel gating currents and thus likely reports on rapid changes in S4 environment (i.e., translocation during depolarization). At more negative potentials, there is a large slow quenching component reflecting fluorophore environment changes relative to the rest of the voltage sensor (particularly the S1–S2 region) that does not appear to be required for channel opening to occur and persists well after ionic current has reached its peak. Reversal of this slow change matches the voltage dependence and time course of channel deactivation and appears to be rate limiting for channel closure. This is the first report of such a slow protein movement within the voltage-sensing domain and highlights both potential differences in channel gating between Kv1.2 and other Kv1 channels and the involvement/motion of the entire Kv1.2 voltage-sensing domain during activation.

We wish to thank Dr. Zhuren Wang for assistance with gating current measurements, Dr. David Steele for help with designing the chimera constructs, and Ka Kee Chiu and Kyung Hee Park for assistance with cell culture.

This work was supported by grants from the Heart and Stroke Foundation of British Columbia and Yukon and the Canadian Institutes of Health Research to D. Fedida. A.J. Horne was supported by a postgraduate scholarship from the Natural Sciences and Engineering Research Council of Canada.

Edward N. Pugh Jr. served as editor.

Submitted: 4 February 2010
Accepted: 27 May 2010

REFERENCES

Baker, O.S., H.P. Larsson, L.M. Mannuzzu, and E.Y. Isacoff. 1998. Three transmembrane conformations and sequence-dependent displacement of the S4 domain in *Shaker* K^+ channel gating. *Neuron.* 20:1283–1294. doi:10.1016/S0896-6273(00)80507-3

Cha, A., and F. Bezanilla. 1997. Characterizing voltage-dependent conformational changes in the *Shaker* K^+ channel with fluorescence. *Neuron.* 19:1127–1140. doi:10.1016/S0896-6273(00)80403-1

Cha, A., and F. Bezanilla. 1998. Structural implications of fluorescence quenching in the *Shaker* K^+ channel. *J. Gen. Physiol.* 112:391–408. doi:10.1085/jgp.112.4.391

Chen, F.S., D. Steele, and D. Fedida. 1997. Allosteric effects of permeating cations on gating currents during K^+ channel deactivation. *J. Gen. Physiol.* 110:87–100. doi:10.1085/jgp.110.2.87

Claydon, T.W., M. Vaid, S. Rezazadeh, S.J. Kehl, and D. Fedida. 2007a. 4-aminopyridine prevents the conformational changes associated with p/c-type inactivation in *Shaker* channels. *J. Pharmacol. Exp. Ther.* 320:162–172. doi:10.1124/jpet.106.110411

Claydon, T.W., M. Vaid, S. Rezazadeh, D.C. Kwan, S.J. Kehl, and D. Fedida. 2007b. A direct demonstration of closed-state inactivation of K^+ channels at low pH. *J. Gen. Physiol.* 129:437–455. doi:10.1085/jgp.200709774

Doyle, D.A., J. Morais Cabral, R.A. Pfuetzner, A.L. Kuo, J.M. Gulbis, S.L. Cohen, B.T. Chait, and R. MacKinnon. 1998. The structure of the potassium channel: molecular basis of K^+ conduction and selectivity. *Science.* 280:69–77. doi:10.1126/science.280.5360.69

Fedida, D., R. Bouchard, and F.S.P. Chen. 1996. Slow gating charge immobilization in the human potassium channel Kv1.5 and its prevention by 4-aminopyridine. *J. Physiol.* 494:377–387.

Gandhi, C.S., E. Loots, and E.Y. Isacoff. 2000. Reconstructing voltage sensor-pore interaction from a fluorescence scan of a voltage-gated K^+ channel. *Neuron.* 27:585–595. doi:10.1016/S0896-6273(00)00068-4

Haitin, Y., I. Yisharel, E. Malka, L. Shamgar, H. Schottelndreier, A. Peretz, Y. Paas, and B. Attali. 2008. S1 constrains S4 in the voltage sensor domain of Kv7.1 K+ channels. *PLoS One.* 3:e1935. doi:10.1371/journal.pone.0001935

Hesketh, J.C., and D. Fedida. 1999. Sequential gating in the human heart $K(^+)$ channel Kv1.5 incorporates Q(1) and Q(2) charge components. *Am. J. Physiol.* 277:H1956–H1966.

Hoshi, T., W.N. Zagotta, and R.W. Aldrich. 1991. Two types of inactivation in *Shaker* K^+ channels: effects of alterations in the carboxy-terminal region. *Neuron.* 7:547–556. doi:10.1016/0896-6273(91)90367-9

Jiang, Y., A. Lee, J. Chen, V. Ruta, M. Cadene, B.T. Chait, and R. MacKinnon. 2003. X-ray structure of a voltage-dependent K+ channel. *Nature.* 423:33–41. doi:10.1038/nature01580

Jogini, V., and B. Roux. 2007. Dynamics of the Kv1.2 voltage-gated K+ channel in a membrane environment. *Biophys. J.* 93:3070–3082. doi:10.1529/biophysj.107.112540

Koopmann, R., A. Scholle, J. Ludwig, T. Leicher, T. Zimmer, O. Pongs, and K. Benndorf. 2001. Role of the S2 and S3 segment in determining the activation kinetics in Kv2.1 channels. *J. Membr. Biol.* 182:49–59.

Larsson, H.P., O.S. Baker, D.S. Dhillon, and E.Y. Isacoff. 1996. Transmembrane movement of the *Shaker* K^+ channel S4. *Neuron.* 16:387–397. doi:10.1016/S0896-6273(00)80056-2

Lee, S.Y., A. Banerjee, and R. MacKinnon. 2009. Two separate interfaces between the voltage sensor and pore are required for the function of voltage-dependent K(+) channels. *PLoS Biol.* 7:e47. doi:10.1371/journal.pbio.1000047

Lewis, A., V. Jogini, L. Blachowicz, M. Lainé, and B. Roux. 2008. Atomic constraints between the voltage sensor and the pore domain in a voltage-gated K^+ channel of known structure. *J. Gen. Physiol.* 131:549–561. doi:10.1085/jgp.200809962

Li-Smerin, Y., and K.J. Swartz. 2001. Helical structure of the COOH terminus of S3 and its contribution to the gating modifier toxin receptor in voltage-gated ion channels. *J. Gen. Physiol.* 117:205–218. doi:10.1085/jgp.117.3.205

Li-Smerin, Y., D.H. Hackos, and K.J. Swartz. 2000. α-Helical structural elements within the voltage-sensing domains of a K^+ channel. *J. Gen. Physiol.* 115:33–50. doi:10.1085/jgp.115.1.33

Long, S.B., E.B. Campbell, and R. Mackinnon. 2005a. Crystal structure of a mammalian voltage-dependent *Shaker* family K^+ channel. *Science.* 309:897–903. doi:10.1126/science.1116269

Long, S.B., E.B. Campbell, and R. Mackinnon. 2005b. Voltage sensor of Kv1.2: structural basis of electromechanical coupling. *Science.* 309:903–908. doi:10.1126/science.1116270

Long, S.B., X. Tao, E.B. Campbell, and R. MacKinnon. 2007. Atomic structure of a voltage-dependent K+ channel in a lipid membrane-like environment. *Nature.* 450:376–382. doi:10.1038/nature06265

Loots, E., and E.Y. Isacoff. 1998. Protein rearrangements underlying slow inactivation of the *Shaker* K^+ channel. *J. Gen. Physiol.* 112:377–389. doi:10.1085/jgp.112.4.377

Loots, E., and E.Y. Isacoff. 2000. Molecular coupling of S4 to a K^+ channel's slow inactivation gate. *J. Gen. Physiol.* 116:623–636. doi:10.1085/jgp.116.5.623

Mannuzzu, L.M., M.M. Moronne, and E.Y. Isacoff. 1996. Direct physical measure of conformational rearrangement underlying potassium channel gating. *Science.* 271:213–216. doi:10.1126/science.271.5246.213

Olcese, R., R. Latorre, L. Toro, F. Bezanilla, and E. Stefani. 1997. Correlation between charge movement and ionic current during slow inactivation in *Shaker* K^+ channels. *J. Gen. Physiol.* 110:579–589. doi:10.1085/jgp.110.5.579

Pathak, M.M., V. Yarov-Yarovoy, G. Agarwal, B. Roux, P. Barth, S. Kohout, F. Tombola, and E.Y. Isacoff. 2007. Closing in on the resting state of the *Shaker* $K(^+)$ channel. *Neuron.* 56:124–140. doi:10.1016/j.neuron.2007.09.023

Paulmichl, M., P. Nasmith, R. Hellmiss, K. Reed, W.A. Boyle, J.M. Nerbonne, E.G. Peralta, and D.E. Clapham. 1991. Cloning and expression of a rat cardiac delayed rectifier potassium channel. *Proc. Natl. Acad. Sci. USA.* 88:7892–7895. doi:10.1073/pnas.88.17.7892

Peters, C.J., M. Vaid, A.J. Horne, D. Fedida, and E.A. Accili. 2009. The molecular basis for the actions of KVbeta1.2 on the opening and closing of the KV1.2 delayed rectifier channel. *Channels (Austin).* 3:314–322.

Rezazadeh, S., H.T. Kurata, T.W. Claydon, S.J. Kehl, and D. Fedida. 2007. An activation gating switch in Kv1.2 is localized to a threonine residue in the S2-S3 linker. *Biophys. J.* 93:4173–4186. doi:10.1529/biophysj.107.116160

Russell, S.N., N.G. Publicover, P.J. Hart, A. Carl, J.R. Hume, K.M. Sanders, and B. Horowitz. 1994. Block by 4-aminopyridine of a Kv1.2 delayed rectifier K^+ current expressed in *Xenopus* oocytes. *J. Physiol.* 481:571–584.

Savalli, N., A. Kondratiev, L. Toro, and R. Olcese. 2006. Voltage-dependent conformational changes in human $Ca(^{2+})$- and voltage-activated $K(^+)$ channel, revealed by voltage-clamp fluorometry. *Proc. Natl. Acad. Sci. USA.* 103:12619–12624. doi:10.1073/pnas.0601176103

Seoh, S.A., D. Sigg, D.M. Papazian, and F. Bezanilla. 1996. Voltage-sensing residues in the S2 and S4 segments of the *Shaker* K^+ channel. *Neuron.* 16:1159–1167. doi:10.1016/S0896-6273(00)80142-7

Smith, P.L., and G. Yellen. 2002. Fast and slow voltage sensor movements in HERG potassium channels. *J. Gen. Physiol.* 119:275–293. doi:10.1085/jgp.119.3.275

Vaid, M., T.W. Claydon, S. Rezazadeh, and D. Fedida. 2008. Voltage clamp fluorimetry reveals a novel outer pore instability in a mammalian voltage-gated potassium channel. *J. Gen. Physiol.* 132:209–222. doi:10.1085/jgp.200809978

Vaid, M., A. Horne, T. Claydon, and D. Fedida. 2009. Rapid outer pore movements after opening in a KV1 potassium channel are revealed by TMRM fluorescence from the S3-S4 linker, and modulated by extracellular potassium. *Channels (Austin).* 3:3–5.

Villalba-Galea, C.A., W. Sandtner, D.M. Starace, and F. Bezanilla. 2008. S4-based voltage sensors have three major conformations. *Proc. Natl. Acad. Sci. USA.* 105:17600–17607. doi:10.1073/pnas.0807387105

Wang, M.H., S.P. Yusaf, D.J.S. Elliott, D. Wray, and A. Sivaprasadarao. 1999. Effect of cysteine substitutions on the topology of the S4 segment of the *Shaker* potassium channel: implications for molecular models of gating. *J. Physiol.* 521:315–326. doi:10.1111/j.1469-7793.1999.00315.x

Watanabe, I., J. Zhu, J.J. Sutachan, A. Gottschalk, E. Recio-Pinto, and W.B. Thornhill. 2007. The glycosylation state of Kv1.2 potassium channels affects trafficking, gating, and simulated action potentials. *Brain Res.* 1144:1–18. doi:10.1016/j.brainres.2007.01.092

Yarov-Yarovoy, V., D. Baker, and W.A. Catterall. 2006. Voltage sensor conformations in the open and closed states in ROSETTA structural models of K(+) channels. *Proc. Natl. Acad. Sci. USA.* 103:7292–7297. doi:10.1073/pnas.0602350103

Yusaf, S.P., D. Wray, and A. Sivaprasadarao. 1996. Measurement of the movement of the S4 segment during the activation of a voltage-gated potassium channel. *Pflugers Arch.* 433:91–97. doi:10.1007/s004240050253

Zhu, J., I. Watanabe, A. Poholek, M. Koss, B. Gomez, C. Yan, E. Recio-Pinto, and W.B. Thornhill. 2003. Allowed N-glycosylation sites on the Kv1.2 potassium channel S1-S2 linker: implications for linker secondary structure and the glycosylation effect on channel function. *Biochem. J.* 375:769–775. doi:10.1042/BJ20030517